



**4-th International Meeting on
Cavitation and Dynamic Problems in Hydraulic Machinery and Systems,
October, 26-28, 2011, Belgrade, Serbia**

Identification by CFD Simulation of the Mechanism Inducing Upper Part Load Resonance Phenomenon

Sébastien Alligné¹, Christophe Nicolet² and François Avellan¹

¹Laboratory for Hydraulic Machines, EPFL

Av. de Cour 33 bis, Lausanne, CH-1007, Switzerland, sebastien.alligne@epfl.ch, francois.avellan@epfl.ch

²Power Vision Engineering sàrl

Ch. des Champs-Courbes 1, Ecublens, CH-1024, Switzerland, Christophe.nicolet@powervision-eng.ch

Abstract

Under part load operation, the swirling flow leaving the Francis turbine runner induces pressure fluctuations featuring fundamental frequency in the range of 0.2 to 0.4 times the runner rotational frequency. The precession of the cavitation vortex rope is an excitation source for the whole hydraulic system. The frequency of the excitation may match with one of the eigenfrequency of the system leading to resonance phenomena. For the upper part load operation range, pressure surge fluctuations may occur in a higher frequency range between 2 and 4 times the runner frequency and may feature modulations at the vortex rope precession frequency. Nowadays the mechanism being able to induce this upper part load resonance is still unknown. Some authors explain this phenomenon as the response of the hydraulic system to periodic impacts of the vortex rope on the inner elbow part of the draft tube, whereas others assume that it is related to the self rotation of the cavitation vortex core featuring an elliptical cross section. In this paper, authors bring some answers to explain this phenomenon with the help of flow numerical simulations of the cavitation vortex rope. It brings out that the root cause is an instability of the cavitation volume which fluctuates at the undesirable frequency matching with one of the eigenfrequency of the hydraulic system. The case study is the FLINDT reduced scale model installed on the EPFL test rig where upper part load resonance phenomenon occurred. This cavitation volume instability is captured with two phase simulations which reveal an elliptical shape of the vortex core as well. However, the phenomenon occurs at a Thoma number much higher than the one obtained by measurements. Therefore, the cavitation volume is very small compared to the experiments. Despite of this offset, a hydroacoustic simulation of the upper part load resonance is performed. A one dimensional hydroacoustic draft tube model including three key parameters is used: the excitation momentum source corresponding to the force induced by the vortex rope on the wall, the excitation mass source induced by the cavitation volume fluctuations and the thermodynamic damping modeling energy dissipation during the phase change between cavitation and liquid. These hydroacoustic parameters are derived from flow numerical simulations and applied to the hydroacoustic model of the hydraulic system. It brings out that a high order eigenmode of the system is excited by the unstable cavitation volume fluctuation frequency. However, no modulation at the vortex rope frequency is experienced contrary to the experiments.

Keywords: Francis Turbine, Upper part load vortex rope, 3D flow numerical simulations, Cavitation, 1D fluid transients simulations, Resonance.

1. Introduction

With economical energy market strategies based on instantaneous pricings of electricity as function of the demand or the predictions, operators harness more hydroelectric facilities to off-design operating points to cover the variations of the electricity production. Under these conditions, Francis turbine develops a cavitation swirling flow at the runner outlet which induces pressure fluctuations propagating in the whole hydraulic system. The core of this cavitation vortex is usually called vortex rope. At resonance conditions, the superimposition of the induced traveling waves gives birth to a standing wave leading to undesirable large pressure and output power fluctuations. Three kind of pressure surgings can be observed either on reduced scale model or prototype installation, see Dörfler [1]. The first one is observed at part load conditions for low flow rates. The helical vortex rope acts as an external forcing function on the hydraulic system, which precession frequency near 0.3 times the runner frequency n can match with one of the eigenfrequency of the system. The second one is observed at upper part load conditions for flow rates higher than the previous case but still lower than the best efficiency point. The occurrence of this resonance phenomenon is

different to the part load resonance since frequency of pressure and output power fluctuations is much higher between $2n$ and $4n$. This resonance appeared for reduced scale models of high specific speed in a narrow operating range, but not yet observed on prototypes. The third one is observed at full load conditions for high flow rates. The axisymmetric vortex rope acts as an internal energy source leading to instability phenomenon called self excited surge.

In this paper, the upper part load operating condition is numerically investigated in order to identify the mechanism inducing the resonance phenomenon. Experimental, theoretical and numerical investigations were carried out for more than fifteen years to understand this phenomenon. Dörfler was one of the first to try to explain experimentally this pressure surge [2]. Despite of extensive measurements of pressure fluctuations, he suggested a qualitative explanation of inertial waves traveling along the surface of the rotating cavitation volume with high propagation speed. Arpe [3] investigated experimentally this kind of resonance as well, in the framework of the FLINDT project. The pressure fluctuations measurements make apparent in the whole draft tube a characteristic frequency value at $2.5n$. Moreover, a modulation of this frequency with the vortex rope precession frequency is pointed out. By the analysis of the phase shift of the high frequency component $2.5n$, Arpe et al. [4] confirmed Dörfler's explanation. Indeed, they interpreted the phase shift as the time propagation of a pressure wave, which excitation source is located in the elbow. Based on this experimental data, Nicolet et al. [5] explained the excitation source as periodic impacts of the vortex rope on the inner elbow part of the draft tube wall. They modeled this excitation with a momentum source combining sinusoidal pressure fluctuations with periodic dirac impulses both at the precession frequency. The amplitude spectrum of such excitation features energy at the vortex rope precession harmonics. Then, they performed a time domain simulation of the hydraulic system response to this excitation with the SIMSEN software. Finally, resonance was simulated due to a matching between the eigenfrequency of the system at $2.5n$ and one of the harmonics of the excitation source. As a result, a standing wave at $2.5n$ is experienced in the whole hydraulic system which is conflicting with the assumption of a traveling wave set by Arpe et al. [4]. The modeling of the excitation source, based on the shock assumption on the inner elbow part of the draft tube wall, is not shared by Koutnik et al. [6] for two reasons. The first one is that the high frequency component is not obviously a multiple of the vortex rope precession frequency. The second one is that the helical vortex rope may be relatively short and does not reach the draft tube elbow. Based on high speed camera visualizations, these authors believe in another theory being a rotation of the cavitation vortex core on its own axis featuring an elliptical cross section. The frequency of this self rotation is identified at the half of the pressure surge frequency. Habán et al. [7] showed that this elliptical cross section is an eigenmode shape of the cavitation swirling flow. Indeed, they performed a stability analysis of a swirling flow in an infinite cylindrical domain described by the set of equations including the Euler equations, the continuity equation and the Laplace equation dealing with the effect of surface tension on the vortex rope boundary. By computing the eigenvalues and the eigenmodes of this set of equations, they showed the existence of this elliptical shape rotating at a given frequency on its own axis. Then, Pochyly et al. [8] applied this methodology to the FLINDT case study where the draft tube domain is simplified by a divergent straight pipe which longitudinal profile of cross sections corresponds to the real elbow draft tube geometry. They confirmed the same results as Habán et al. [7].

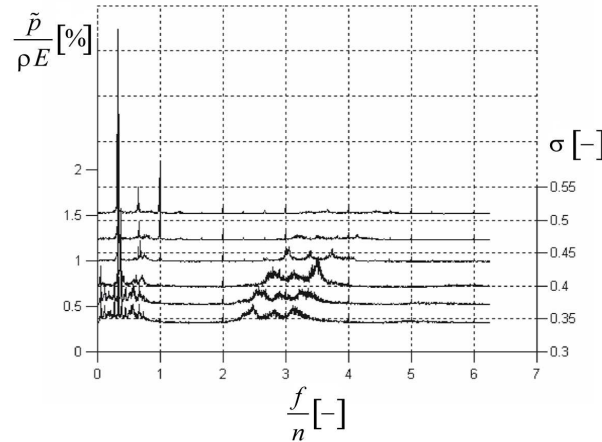
Nowadays the mechanism being able to induce this upper part load resonance is still unknown. As explained previously, some authors explain this phenomenon as the response of the hydraulic system to periodic impacts of the vortex rope on the inner elbow part of the draft tube, whereas others assume that it is related to the self rotation of the cavitation vortex core featuring an elliptical cross section. The aims of this paper are first to bring some answers to explain this phenomenon with the help of 3D flow numerical simulations and then to simulate the hydroacoustic upper part load resonance between the helical vortex rope and the hydraulic system. To reach this purpose, a 3D incompressible flow model, called hydrodynamic (HD) model, is used to identify the excitation source induced by the helical vortex rope. Moreover, a 1D compressible model, called hydroacoustic (HA) model, is used to simulate the propagation of the HA sources derived from the HD model. The first section of this paper presents the measurements of interest, performed on the FLINDT reduced scale model to illustrate the researched phenomenon. Secondly, HA and HD models of the draft tube flow, used for the identification of the excitation sources are described. Then, the mechanism able to induce the upper part load resonance phenomenon is identified by the HA analysis of the simulation results obtained with the HD model. Finally, the time domain simulation of the upper part load resonance is performed.

2. Case study

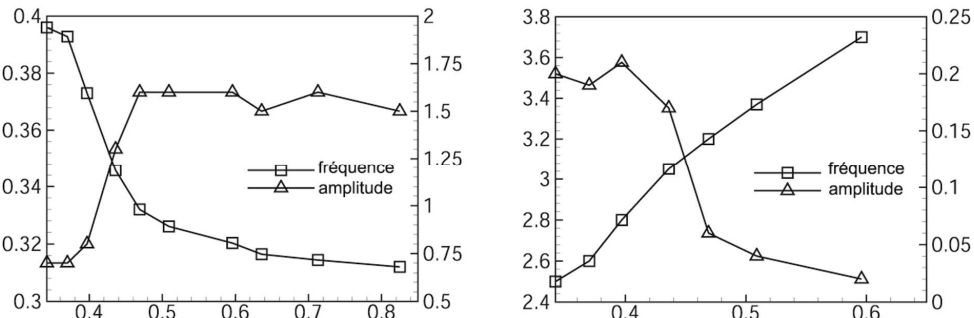
In the framework of the FLINDT project [9], Eureka N° 1625, experimental and numerical investigations have been carried out to achieve a better understanding of the flow pattern in a Francis draft tube. The selected Francis turbine runner features a high specific speed equal to $\nu = 0.56$ and corresponds to the scale model of a hydropower plant built in 1926 owned by ALCAN. The runner has 17 blades with an outlet diameter of 0.4 m. The original draft tube geometry is of Moody type and was replaced for this research project by an elbow draft tube with one pier. This scale model was installed on the third test rig of the EPFL Laboratory for Hydraulic Machines. Among the several contributions, extensive wall pressure fluctuations measurements were performed for different operating points under various Thoma number by Arpe [3]. In order to capture the helical vortex core precession phenomenon in the draft tube, 104 piezoresistive absolute pressure sensors installed in the draft tube wall are acquired with a HP-VXI acquisition system using a sampling frequency equal to sixteen times the runner frequency. The phenomenon of interest is the upper part load resonance which was observed and measured at a low flow rate turbine operating point given in Table 1.

Table 1 Operating point conditions

φ/φ_{BEP}	ψ/ψ_{BEP}	N	GVO	σ
[-]	[-]	[rpm]	[°]	[-]
0.703	1.06	750	16	0.38

**Fig. 1** Influence of the Thoma Number on pressure fluctuations in the cone [3].

Spectral analysis of the pressure fluctuations measured in the cone is presented as function of the Thoma number in Fig. 1. For high Thoma number, the measured pressure fluctuations feature the helical precession frequency near 0.32 times the runner frequency n , called afterwards f_{rope} . Under these cavitation conditions, the excitation induced by the helical vortex rope does not lead to resonance phenomenon. Unsteady flow numerical simulations have been performed at these free cavitation conditions to find out this precession frequency, see Ciocan et al. [10] and Zobeiri [11]. However, by decreasing the Thoma number, pressure fluctuations between $2n$ and $4n$ appear and are modulated by the vortex rope precession. Therefore, three characteristic frequencies can be observed in this frequency range. For this paper, the Thoma number value of $\sigma = 0.38$ is considered. At this condition, the modulated frequency is equal to $2.5n$ leading to pressure fluctuation amplitudes at $2.5n \pm f_{rope}$. During measurements, strong noise and vibration of the draft tube were reported. This phenomenon is called upper part load resonance, but can be encountered without modulation as well [2]. Fig. 2 shows more in details the influence of the Thoma number on the two characteristic frequencies included in pressure fluctuations.

**Fig. 2** Influence of σ on the precessing vortex rope frequency and on the high frequency modulated component [3].

The vortex precession frequency increases slightly by decreasing the Thoma number whereas the higher frequency decreases. Due to the dependence of the characteristic frequencies with the Thoma number, the occurrence of the resonance is very sensitive to the cavitation volume in the draft tube. It can be noticed that pressure fluctuations related to the vortex rope precession are only located in the area of the draft tube cone and elbow, while pressure fluctuations at $2.5n$ are measured in the entire draft tube and in the turbine intake as well [3]. These observations suggest that the precession frequency component is due to the local three dimensional flow in the draft tube whereas the high frequency component at $2.5n$ corresponds to a one dimensional hydroacoustic eigenmode of the hydraulic system responding to the vortex rope excitation. This assumption is confirmed by the analysis of the phase shift between the pressure signals in the draft tube [4]. Pressure pulsations at the vortex rope precession frequency in the same cone cross section are phase shifted each other corresponding to the geometric angle location in the cone. This yields to the conclusion that the precession frequency component is due to the passage of the cavitation vortex core near the pressure sensor. Regarding the higher frequency component at $2.5n$, the phase shift computation is given in an unfolded draft tube representation in the left part of Fig. 3.

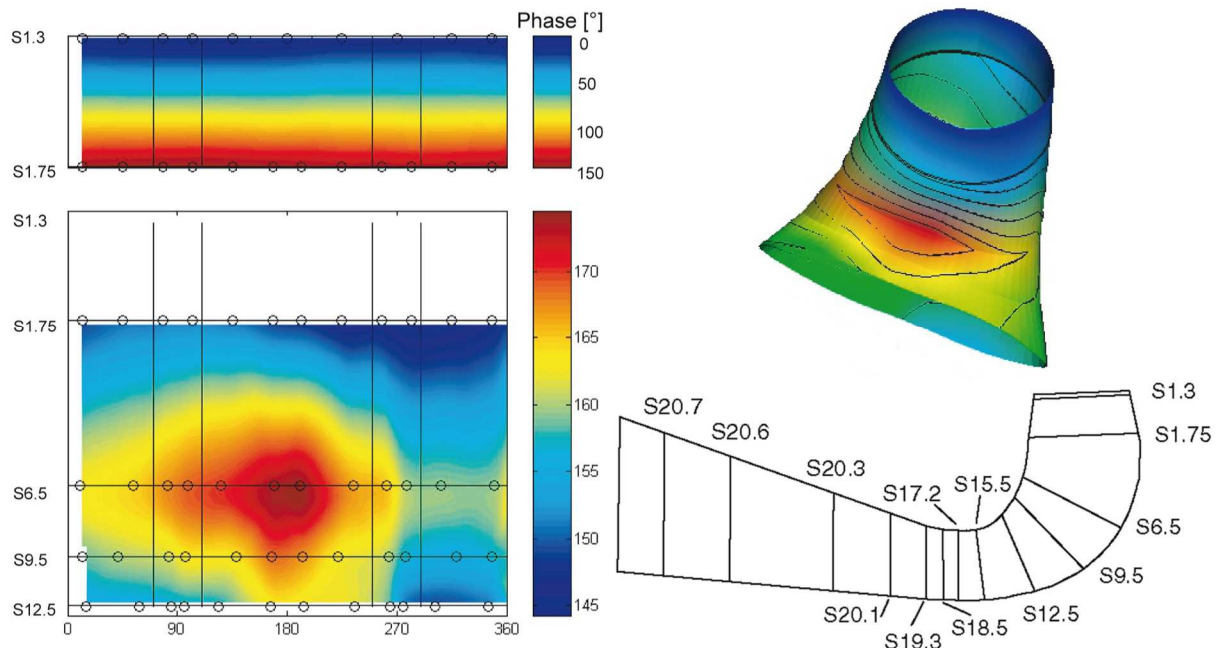


Fig. 3 Phase shift analysis of pressure fluctuations in the draft tube at the high frequency component value of $2.5n$ [3].

In the cone, no phase shift is experienced between pressure signals located in the same cross section. However, a phase shift of 150° is computed between the inlet and the outlet cone. At this stage of the analysis, two assumptions about the nature of these high frequency synchronous pulsations can be set. The first one is that the longitudinal phase shift value of 150° corresponds to the time propagation of a 1D traveling wave in the draft tube [4]. The second one is that this phase shift is due to a 1D standing wave corresponding to an eigenmode of the hydraulic system featuring a pressure node in the cone [5]. In the both cases, the one dimensional property is lost in the elbow due to the curvature.

3. Hydroacoustic draft tube model

The one dimensional HA model of the hydraulic system is set up with the SIMSEN software developed by the EPFL. This software is able to simulate the transient behavior of a complete hydroelectric power plant, [12]. In order to get a common set of differential equations for both electrical and hydraulic parts, hydraulic models are based on the electrical analogy. To model the draft tube component, the two diffusors channels separated by the pier are considered separately from the cone and the elbow parts where it is assumed that cavitation onset is located. For simplicity, the "draft tube" term will be used afterwards to name both the cone and the elbow parts. Therefore, the pier is modeled with a standard viscoelastic pipe model [12] with an equivalent cross section, like the remaining water passages of the whole hydraulic system. With this standard viscoelastic pipe model, the pressure force and the viscous force acting on the wall are modeled respectively with a Taylor development and the Darcy-Weisbach formulation [13]. However, this modeling is inadequate to describe the dynamic behavior of the cavitation vortex rope precession in the draft tube pipe. Hence, fundamental modifications of the standard pipe model are necessary. Alligné et al. [14] proposed a model including a mass source related to the cavitation volume fluctuation, a momentum source representing the forces acting on the draft tube wall and finally a thermodynamic damping modeling the energy dissipation during the phase change between the cavitation and the surrounding liquid. They derived these quantities from 3D flow numerical simulations to be injected into the 1D HA model of the complete hydraulic system. This methodology was applied to simulate the part load resonance phenomenon occurring between the helical vortex rope precession frequency and the first eigenfrequency of the connected hydraulic system. The order of magnitudes of pressure fluctuations of the hydraulic system response were in good agreement with measurements found in the literature. However, direct comparison with measurements was not available to validate this HA parameters identification.

In this paper, the same HA draft tube model and the same identification procedure of the parameters is used. However, the investigated upper part load resonance phenomenon occurs at a higher frequency value than the case study presented by Alligné et al. [14]. Hence, the wave length of the involved resonating eigenmode is much lower, which requires a higher spatial discretization of the HA draft tube model contrary to the lumped model used by Alligné et al. The equivalent electrical scheme of the distributed HA draft tube model, featuring several pressure nodes defined by the capacitances, is illustrated in Fig. 4.

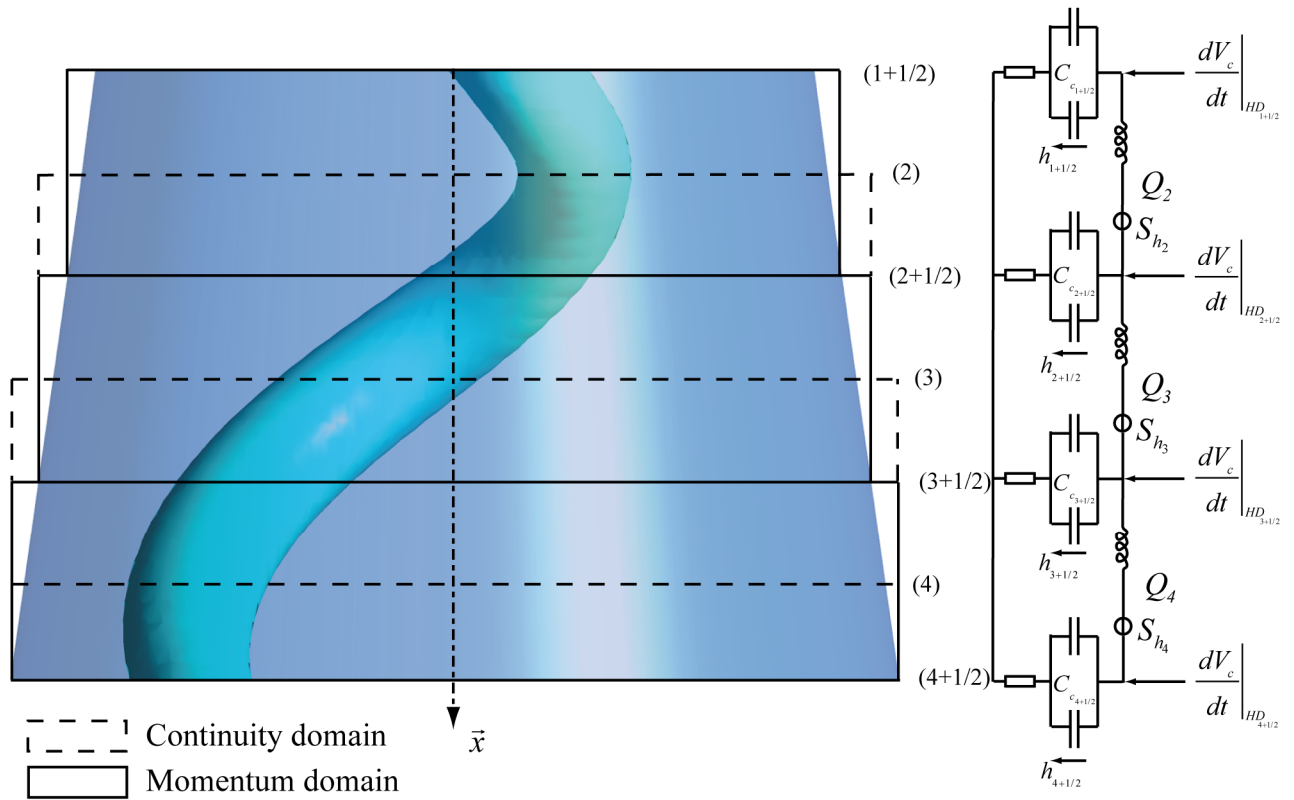


Fig. 4 Spatial discretization required for HA parameters identification [14].

As proposed by Alligné et al., the identification of the electrical components of this model is performed from 3D flow numerical simulations. Therefore, the spatial discretization in the 1D HA model must be reproduced in the 3D computational domain, see Fig. 4. Hence, continuity and momentum control volumes are defined in the 3D HD model to perform continuity and momentum balances which correspond respectively to the node and the mesh equations in the electrical scheme. As a result, nine continuity and ten momentum control volumes are overlapped to describe the whole length of the draft tube including the two diffuser channels. In Fig. 5, the data flow between the 3D HD and the 1D HA draft tube models is shown.

The first set of parameters to be exchanged is the momentum sources S_{h_i} representing the forces induced by the cavitation vortex rope precession acting on the draft tube walls of the different momentum control volumes. Then, the vortex rope cavitation volume fluctuations are considered as mass sources $S_{Q_{i+1/2}}$ for the hydraulic system. Pressure and flow rate fluctuations in the draft tube domain may be split into two components: a HA part due to the propagation waves in the hydraulic system and a HD part due to the incompressible fluid motion [15]:

$$\begin{aligned}
 S_{Q_{i+1/2}} &= S_Q \Big|_{HD_{-j_i}} + S_Q \Big|_{HA_{-j_i}} \\
 &= - \frac{dV_c}{dt} \Big|_{HD_{-j_i}} - \frac{dV_c}{dt} \Big|_{HA_{-j_i}}
 \end{aligned} \tag{1}$$

It is assumed that the HA field can influence dramatically the cavitation volume fluctuation of the vortex rope especially at resonance conditions. The HA feedback on the mass source is modeled to be function of the HA pressure state variable. A linear approximation of this feedback yields to the definition of the equivalent capacitances C_{equ} as follows:

$$C_{equ} = (1 - \beta) C_0 + C_c \tag{2}$$

With C_0 , C_c and β respectively the capacitance in cavitation free conditions, the cavitation compliance parameter and the cavitation volume fraction. As a result, equivalent capacitances C_{equ} and cavitation volume fluctuations due to the HD field $\frac{dV_c}{dt} \Big|_{HD_{-j_i}}$ are exchanged between the HD and the HA draft tube models as illustrated in Fig. 5. These equivalent capacitances

allow to define equivalent wave speeds a_{equ} along the draft tube length according to the following definition of the capacitance:

$$C_{equ} = \frac{gAx}{a_{equ}^2} \tag{3}$$

Finally, the last set of parameters to be exchanged is the thermodynamic dampings μ'' defining the thermodynamic

resistances R_{th} in series with the capacitances to model energy dissipation during the phase change between liquid and cavitation [16]. To get more details on the definition of these exchanged HA parameters, the reader can refer to a previous paper [14].

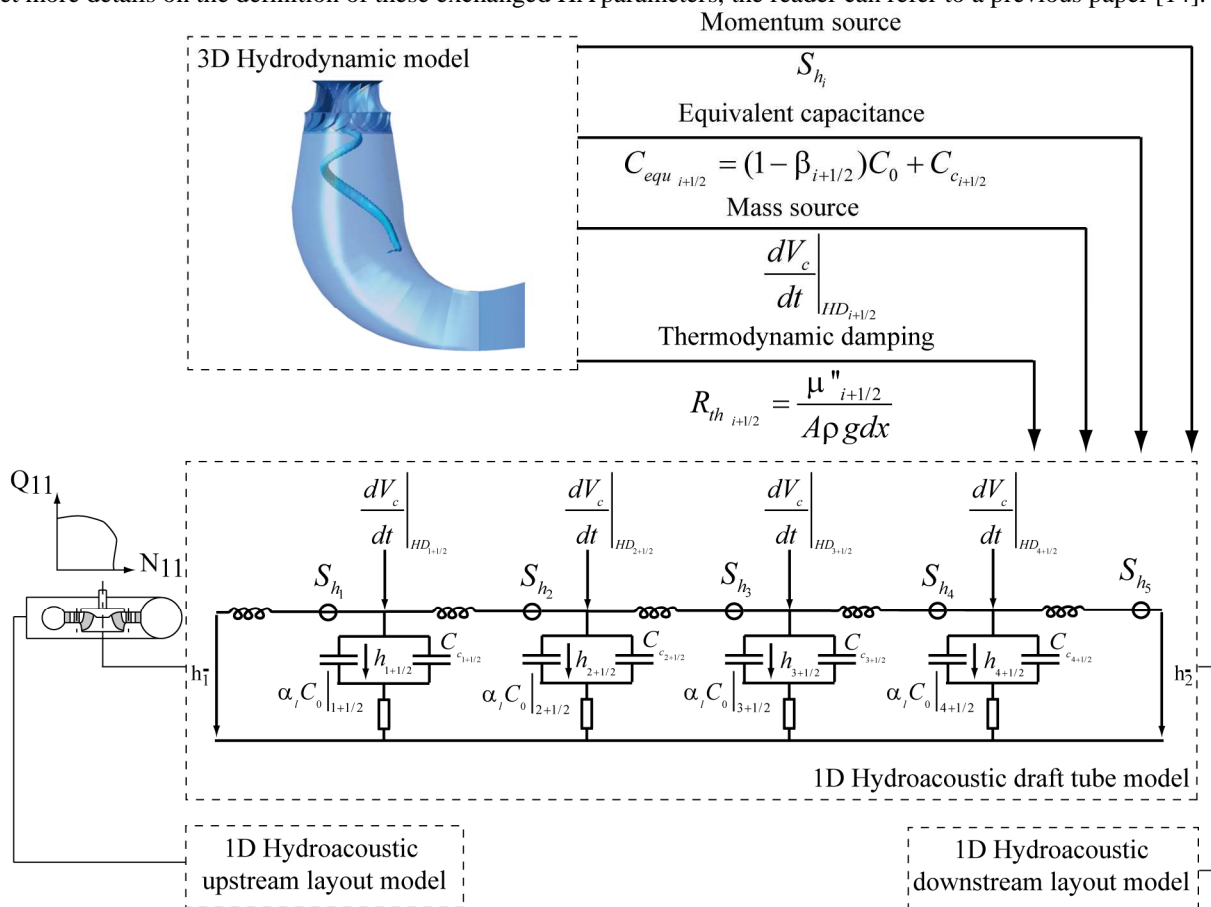


Fig. 5 Data flow between hydroacoustic and hydrodynamic draft tube models.

4. Hydrodynamic draft tube model

For the present application, ANSYS-CFX 12.0 version is used for the computation of the unsteady flow in the FLINDT reduced scale model draft tube. Unsteady Reynolds Averaged Navier-Stokes equations are used. For single phase simulations (SPS), the set of equations is closed with the Scale Adaptive Simulation Shear Stress Transport (SAS-SST) which is a first order two equations turbulence model developed by Menter [17], whereas for two phase simulations (TPS), two turbulence models are compared: the SAS-SST model and the Shear Stress Transport (SST) model. The homogeneous cavitation model adding the transport equation of the void fraction β to the set of equations, is used.

The computational domain is constituted of the runner and the draft tube which is the best compromise between solution accuracy and computer resources. The transient runner-draft tube simulation allows to predict the interaction of the flow between the upstream runner and the elbow draft tube [10], [11]. In Fig. 6, the computational domain is shown with the grid mesh and coloured by the momentum control volumes defined during the mesh generation to derive the momentum sources S_{h_i} .

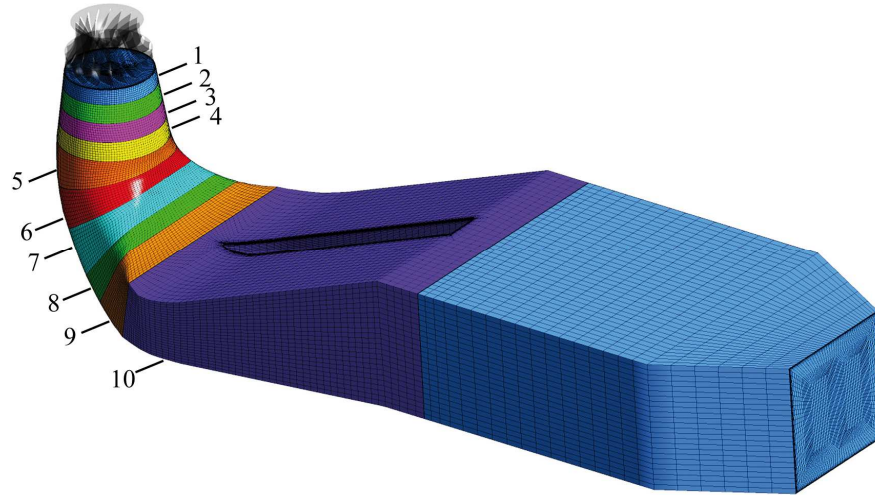


Fig. 6 Grid mesh and momentum control volumes.

A General Grid Interface (GGI) is used between the two components, which interface position is updated for every time step. The computational domain is discretized with a structured mesh of 2.5 million nodes which 1 million for the draft tube component, generated with ANSYS ICEM 12.0. Taking into account this spatial discretization, the "High resolution" advection scheme is used to solve the set of equations. Regarding the time discretization, a time step corresponding to 4° runner revolution is used with the "Second order backward euler" transient scheme. The number of coefficient loops is set to 3 and 30 respectively for single phase and two phase simulations with a RMS convergence criterion of the residual specified to 10^{-4} . The influences of the time step and the space discretization have been extensively studied by Zobeiri [11].

The inlet boundary condition is a prescribed velocity profile at the runner inlet which surface integral gives the flow rate defined by the flow coefficient φ . To define this velocity profile, two preliminary steady simulations were performed [10]. First, steady flow computation in the spiral casing and the distributor is performed. Results are used as inlet conditions for a second steady flow computation in the stay vanes, guide vanes and runner assembly. From that case, inlet conditions for the unsteady computation is extracted at the runner inlet including turbulent kinetic energy and dissipation rate profiles. Regarding the outlet boundary condition, an opening condition with "static pressure for entrainment" is set up. The outlet pressure is prescribed according to the Thoma number investigated, which is a decisive boundary condition for two phase simulations. From the Thoma number definition, the flow and the energy coefficients $\varphi-\psi$ are introduced to derive the pressure at the pier outlet:

$$P_{\bar{t}} = \rho \cdot \psi \cdot \frac{U_{\bar{t}}^2}{2} \cdot \sigma + p_v + \rho g (Z_{ref} - Z_{\bar{t}}) - \rho \cdot \varphi^2 \cdot \frac{U_{\bar{t}}^2 \cdot A_{\bar{t}}^2}{2 \cdot A_{\bar{t}}^2} \quad (4)$$

5. Identification of cavity volume instability

The cavitation volume of the vortex rope is a decisive quantity to derive the HA draft tube parameters. In the case of single phase simulations, the cavitation volume is assumed to correspond to the flow region bounded by the vapor pressure p_v set to 2338 Pa at 20°C . However, for two phase simulations, the state variable of the 3D HD model called vapor volume fraction β is integrated over a specified volume on which the user wants to assess the cavitation volume V_c :

$$V_c = \int_v \beta dV \quad (5)$$

By applying the outlet pressure derived from Eq. (4) corresponding to the investigated Thoma number of $\sigma = 0.38$, no cavitation volume can be observed contrary to experiments. Hence, an offset on this outlet pressure has been applied to fulfill two conditions. First, to get a cavitation volume qualitatively in agreement with experimental visualization and then to obtain a vortex rope precession frequency which matches the best with the experimental measurements. This offset can be formulated as follows:

$$\frac{\sigma_{sim}}{\sigma_{exp}} = 0.59 \quad (6)$$

For convenience, the Thoma number used for numerical simulations is systematically corrected by this factor. Therefore, the subscript *sim* will be omitted afterwards. In Fig. 7, the vortex rope precession frequency obtained by numerical simulations is plotted as function of the corrected Thoma number.

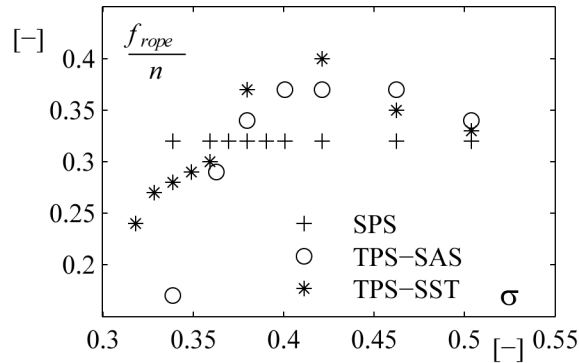


Fig. 7 Vortex rope frequency as function of the Thoma number [14].

For single phase simulations, the frequency is constant and equal to $0.32n$ whereas for two phase simulations the frequency is influenced by the Thoma number as observed experimentally. At the investigated experimental cavitation conditions corresponding to a Thoma number value of 0.38 , the precession frequency is respectively equal to $0.34n$ and $0.37n$ for the two phase simulations with SAS-SST and SST turbulence models. Hence, when cavitation occurs in the vortex core, the precession frequency is higher than the cavitation free case which is in good agreement with experimental measurements, see Fig. 2.

Considering the experimental investigated Thoma number value of 0.38 , the spectral analysis of the HA sources, derived from both single phase and two phase simulations, does not bring out any characteristic frequency near $2.5n$. Neither periodic impacts nor self rotation vortex rope core able to induce this frequency, have been identified at this cavitation condition by the analysis of the HA sources. However, the elliptical shape is well captured in the case of two phase simulations, see [14]. Since the phenomenon is very sensitive to the Thoma number, the HA sources have been computed for different cavitation conditions. The occurrence of a frequency component near $2.5n$ in the HA sources, has been found when two phase simulations combined with the SST turbulence model are considered. However, the SAS-SST turbulence model does not allow to capture this high frequency component. In Fig. 8, the amplitude spectra of the global momentum source, corresponding to the sum of the elementary sources S_{h_i} derived from a two phase simulation with the SST turbulence model, are plotted in a waterfall diagram as function of the Thoma number.

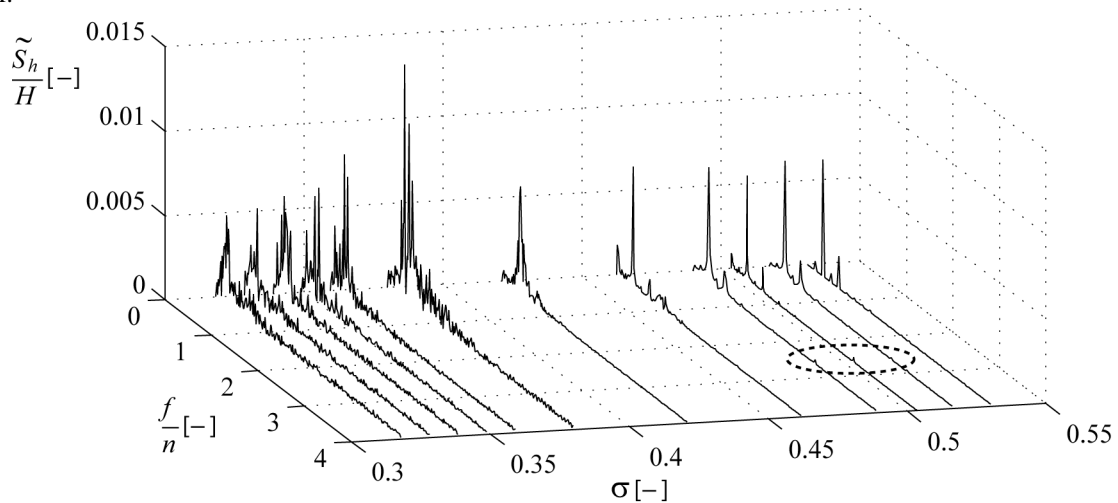


Fig. 8 Influence of σ on the global momentum source.

These amplitude spectra are computed over a time simulation corresponding to 60 runner revolutions. For the low Thoma numbers where cavitation volume is higher than for high Thoma numbers, the amplitude spectra are much noisier due to the unsteadiness of the cavitation. A high frequency component at $2.6n$ appears for Thoma number values between 0.49 and 0.52 . However, this range is higher than the experimental data inducing a smaller cavitation volume than the one observed experimentally. A focus on the Thoma number value of 0.504 is performed to identify the cause of the onset of this high frequency component since its amplitude is found to be maximum at this cavitation domain. In Fig. 9, a waterfall diagram of the amplitude spectra of the momentum sources considered along the draft tube domain is plotted.

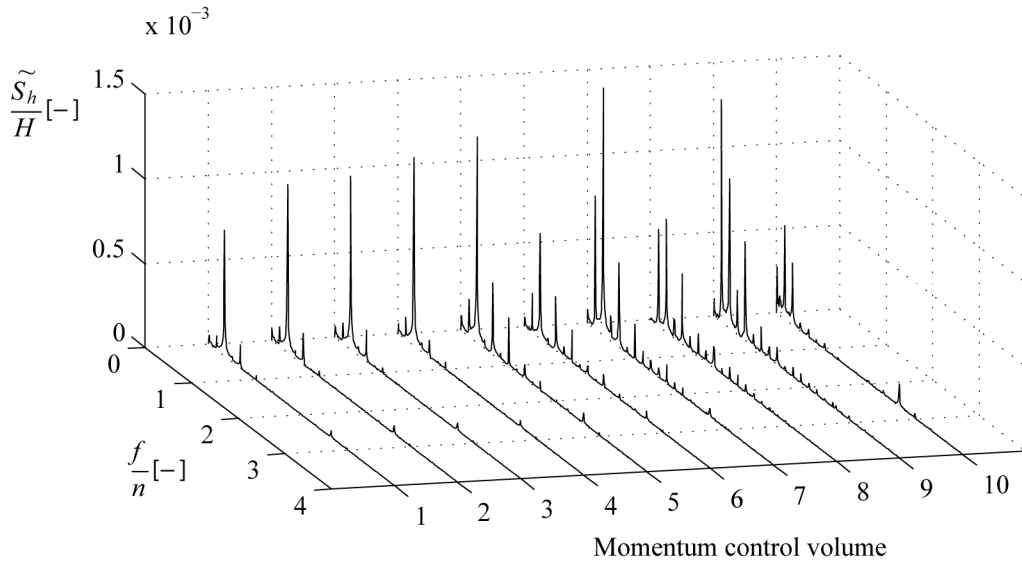


Fig. 9 Waterfall diagram of the amplitude spectra of the momentum sources S_h along the draft tube domain at $\sigma = 0.504$.

The high frequency component is found in the whole draft tube domain. To identify the physical meaning of this high frequency component, the downstream flow rate fluctuations at the elbow outlet cross section Q_2 are monitored. In this cross section no cavitation is experienced by numerical simulations. In Fig. 10, the amplitude spectrum of the outlet flow rate fluctuations normalized by the inlet runner flow rate Q_1 is plotted and compared to the one of the global mass source corresponding to the total cavitation volume fluctuations.

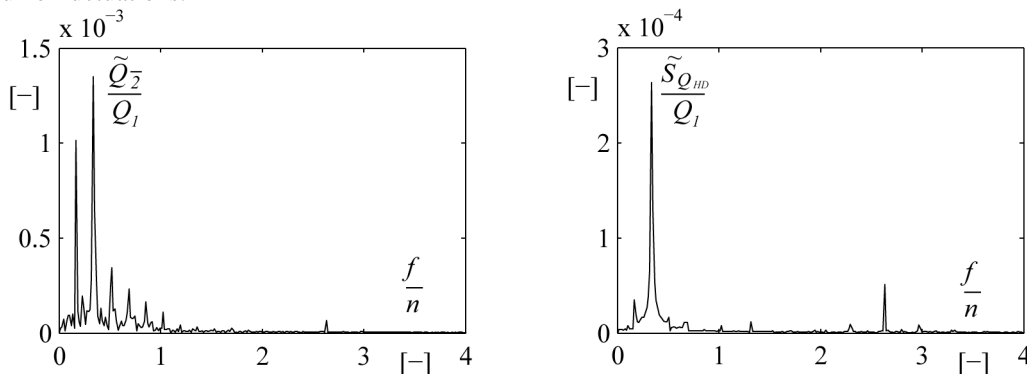


Fig. 10 Amplitude spectra of the outlet discharge Q_2 fluctuations and mass source $S_{Q_{HD}}$ fluctuations.

The outlet flow rate features fluctuations at the high frequency component. However, the prescribed inlet flow rate of the HD model at the runner inlet Q_1 is constant. By applying the continuity equation to a control volume defined between the runner inlet and the elbow outlet it yields to:

$$Q_1 - Q_2 = - \left. \frac{dV_c}{dt} \right|_{HD} = S_{Q_{HD}} \quad (7)$$

Since the inlet flow rate is constant in the HD model, the downstream flow rate fluctuations are due to the cavitation volume fluctuations, shown in Fig. 10 by the amplitude spectrum of the global mass source which features this high frequency component as well. Therefore, the mechanism inducing upper part load resonance with the hydraulic system is identified to be related to a cavitation volume instability which under cavitation conditions, experiences fluctuations at an undesirable frequency which could match with an eigenfrequency of the system.

6. Upper part load resonance simulation

6.1 Computation of HA draft tube model parameters

The cavitation volume instability, which can induce upper part load resonance phenomenon, occurs at a high Thoma number compared to the experiments. Therefore, the simulation of this resonance is not feasible with the HA parameters derived at this high Thoma number. Indeed, the small cavitation amount in the vortex core does not allow to reduce enough the eigenfrequencies of the system to match with the excitation frequency induced by the cavitation volume instability. The aim of this Section is to simulate the upper part load resonance using the HA draft tube model parameters derived from the HD model set up at the same

Thoma number as the experiments. Therefore, the procedure consists in modifying these parameters to model the cavitation volume instability which should have been simulated at this cavitation condition. Then, a one way simulation is carried out by injecting, as a post processing step, the time histories of these modified HA draft tube model parameters in the HA model of the complete hydraulic system. The logic would be to use the parameters derived from the two phase simulation results obtained with the SST turbulence model since it corresponds to the configuration where the cavitation volume instability has been observed. However, using this configuration, HA simulation is numerically unstable because of a critical ratio between the equivalent capacitance parameters C_{equ} and the thermodynamic dampings μ'' . Finally, the modeling of the cavitation volume instability has been integrated to the HA parameters derived from single phase simulation.

This modeling is based on the results obtained at the high Thoma number value of 0.504. It has been found that a fluctuation of 1 % of the time averaged cavitation volume induces a fluctuation of the HA momentum sources in each momentum control volume near 0.005 % of the turbine head. This ratio is taken as a reference to create a relation between cavitation volume fluctuation amplitude and momentum sources fluctuation amplitudes. Then, the amplitude of the cavitation volume fluctuation is taken as a parameter and an "optimal" value is determined in order to get amplitudes of pressure fluctuations at the high frequency component in agreement with measurements. In Fig. 11, the time histories of the modeled cavitation volume fluctuations and the corresponding momentum source fluctuations are plotted.

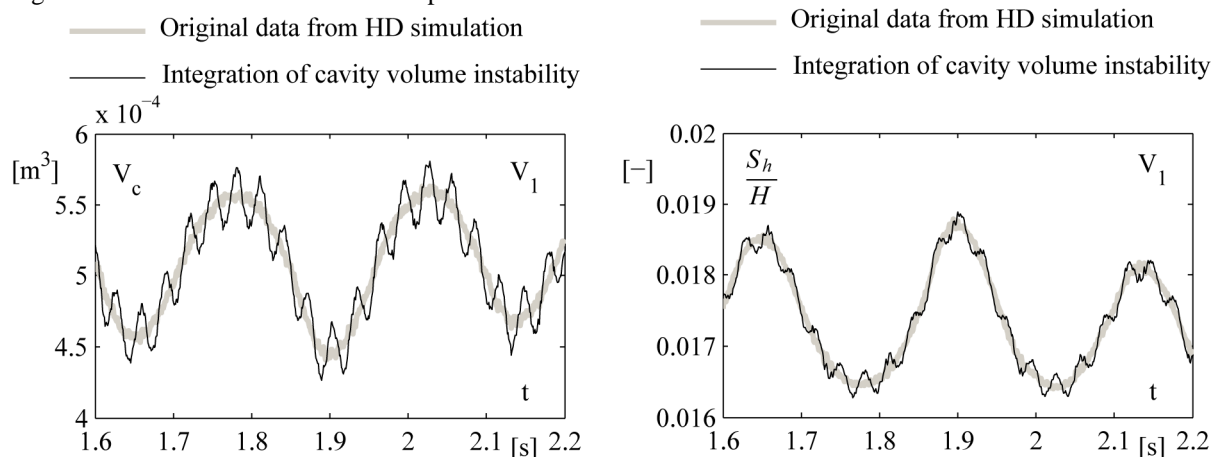


Fig. 11 Integration of the cavitation volume instability to the simulation results with the HD model in the first control volume V_1 .

The amplitude of the cavitation volume fluctuations at the high frequency component, which has been integrated into the original numerical data, corresponds to 15 % of the time averaged cavitation volume. The computation of the equivalent capacitance parameter C_{equ} is derived from the computation of an equivalent wave speed, see Eq. (3), which is estimated from a mathematical model based on an one dimensional approach to the flow of a liquid gas mixture developed by Rath [18]:

$$a_{equ} = \left[\left(\beta \rho_c \frac{p}{p_0} + (1-\beta) \rho \left(1 + \frac{1}{E_l} (p - p_0) \right) \right) \cdot \left(\frac{\beta}{p} + \frac{1-\beta}{E_l} + \frac{D}{e \cdot E_{wall}} \right) \right]^{-\frac{1}{2}} \quad (8)$$

The pressure p in this formulation can be split into two components: a HA part due to the propagation waves and a HD part due to the incompressible fluid motion [15]. However, since a one way simulation is carried out to compute this wave speed, the HA part of the pressure field is not taken into account. Hence a reference pressure of the HD model is considered and set to the outlet pressure of the HD computational domain.

Regarding the bulk viscosity μ'' , modeling the energy dissipation during the phase change between the cavitation and the surrounding liquid, a mathematical model based on a homogeneous flow assumption is used [16]:

$$\mu'' = \frac{\Theta \cdot ((1-\beta) \rho + \beta \rho_c)^2 \cdot \beta \cdot \rho_c \cdot R \cdot T \cdot a_{equ}^4}{p^2} \quad (9)$$

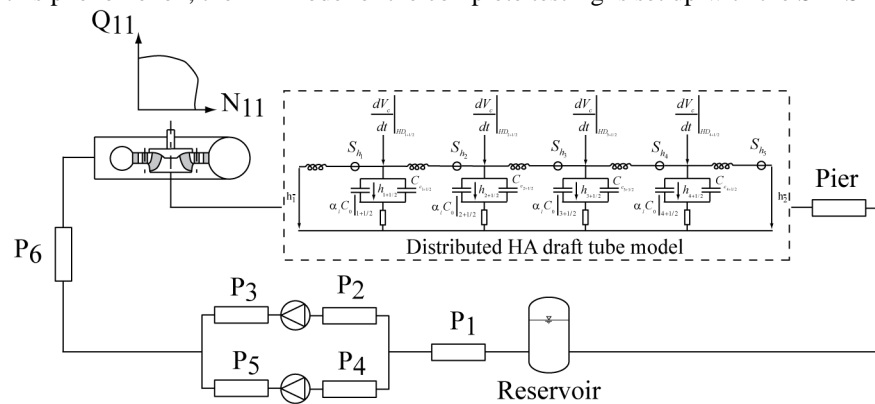
In the same way as the computation of the wave speed, the pressure p in the bulk viscosity formulation is set to the outlet pressure of the HD computational domain. The wave speeds and the bulk viscosities experience fluctuations only due to the cavitation volume fluctuation since the pressure is set as a constant. In Table 2 the time averaged wave speeds and bulk viscosities are given in each continuity control volume.

Table 2 Time averaged wave speeds and bulk viscosities

Continuity control volume	\bar{a}_{equ} [$m.s^{-1}$]	$\bar{\mu}''$ [$Pa.s$]
1	28.8	2'576
2	27.3	2'313
3	28.3	2'486
4	32.6	3'339
5	59.5	10'448
6	138.7	8'968
7	153.6	5'840
8	165.8	608
9	165.6	0

6.2 HA model of the test rig

The upper part load resonance phenomenon was experienced on the third test rig of the EPFL Laboratory for Hydraulic Machines. To investigate this phenomenon, the HA model of the complete test rig is set up with the SIMSEN software, see Fig. 12.

**Fig. 12** Layout of the test rig.

The test rig is a closed loop system with one reservoir and two feed pumps in parallel. The main HA model parameters of the water passages are resumed from a previous model built for the analysis of the upper part load resonance as well, but where it was assumed that the excitation source is periodic impacts on the inner elbow part of the draft tube [5]. To enhance the HA model of the test rig, the turbine characteristic of the Francis turbine runner has been integrated. By setting the HA parameters of the test rig model with the time averaged values, the eigenfrequencies are computed using a small perturbation stability analysis [19], see Table 3. This analysis is based on the computation of the eigenvalues and the eigenvectors of the set of differential equations in SIMSEN which give respectively the eigenfrequencies and the eigenmode shape.

Table 3 Eigenfrequencies of the test rig

Eigenmode order	f/n [-]
1	0.52
2	0.69
3	1.24
4	1.83
5	1.91
6	2.62

The first eigenmode features a frequency higher than the vortex rope precession at $0.32n$. Hence, the standard part load resonance between the vortex rope precession frequency and the first eigenmode can't occur in these cavitation conditions. However, the cavitation volume instability modeled at a frequency value of $2.6n$ will induce resonance with the sixth eigenmode which spatial shape is given in Fig. 13.

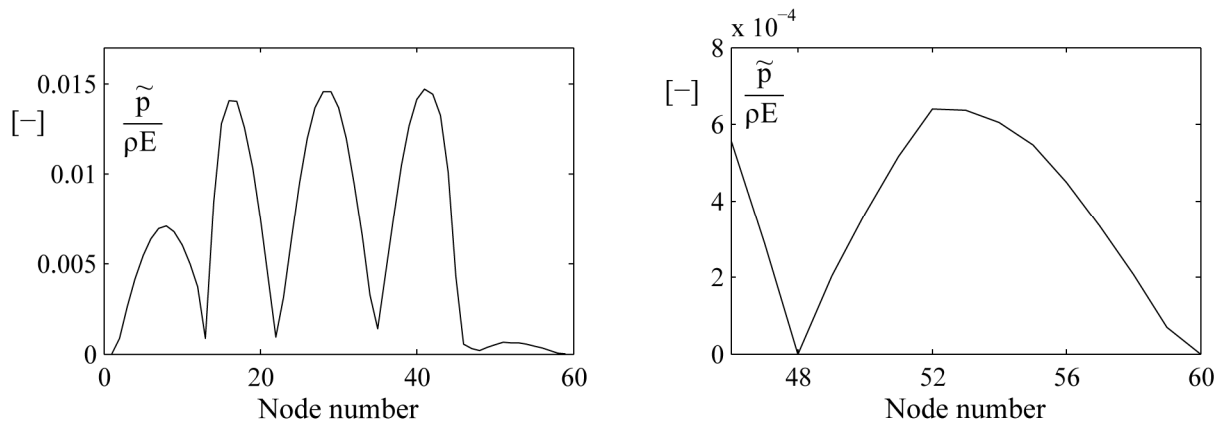


Fig. 13 Shape of the sixth eigenmode in the whole hydraulic system (left) and in the draft tube component (right).

In the left part of Fig. 13, the eigenmode shape is plotted in the whole hydraulic system where the first and the last nodes correspond to the reservoir location. In the right part, the shape is plotted in the draft tube component including the cone, the elbow and the pier. The plotted pressure variable corresponds to the modulus of the complex eigenvectors which explains positive fluctuations in the whole system. However, the phases of these fluctuations are given by the argument of the eigenvectors. Due to the modeling approach which neglects the convective terms in the set of equations, the phase can only reach $\pm\pi$ values. At each pressure node, the phase changes to the opposite value. In the cone and the elbow parts, a pressure node is experienced which is in good agreement with experimental measurements showing a phase shift of 150° between the inlet and the outlet cone pressure fluctuations, see Fig. 3.

6.3 Simulation results

After the integration of the cavitation volume instability in the HA parameters computed at the investigated Thoma number value of 0.38, a one way simulation is carried out. The response of the hydraulic system to the excitation induced by the cavitation vortex rope is represented in Fig. 14.

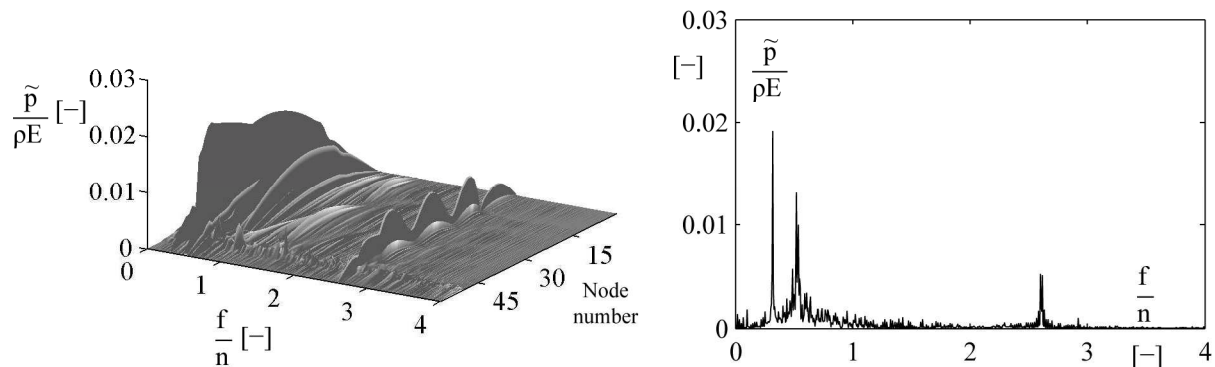


Fig. 14 Surface representation of amplitude spectra pressure fluctuations as function of the position in the hydraulic system (left) and pressure fluctuations in the draft tube cone (right).

In the left part, the surface representation is built from the amplitude spectra pressure fluctuations plotted at each pressure node of the HA model. The draft tube component is located between the node numbers 46 and 60. In the right part, the amplitude spectrum of pressure fluctuations in the draft tube cone is plotted. One can observe that the sixth eigenmode responds to the excitation due to the cavitation volume instability. However, the first eigenmode characterized by a frequency of $0.52n$, responds as well contrary to the measurements. This is due to one of the harmonics of the vortex rope precession frequency which matches with the first eigenfrequency fluctuating because of the unsteadiness of the wave speed parameter. Moreover, the modulation of the hydraulic system response is not simulated.

7. Conclusion

This paper contributes to the understanding of the mechanism inducing upper part load resonance between the cavitating vortex rope and the hydraulic system. A methodology to compute the hydroacoustic parameters of a part load vortex rope model from incompressible flow numerical simulations is presented. Two excitation sources are considered: a momentum one corresponding to the force induced by the vortex rope precession on the draft tube wall and a mass source corresponding to the cavitation volume fluctuations. The analysis of these hydroacoustic sources allowed to explain the phenomenon as an instability of the cavitation volume which fluctuates at the undesirable frequency matching with one of the eigenfrequency of the hydraulic system. The simulation of this cavitation volume instability is very sensitive to the numerical set up. Two phase flow numerical

simulations must be considered and the choice of the turbulence model is decisive. The elliptical shape of the cavitation vortex rope core is well simulated using the homogeneous cavitation model. However, the volume instability at the high frequency component occurs at a Thoma number much higher than the one obtained by measurements.

Acknowledgments

The authors would like to thank particularly Alstom Power for their financial support and assistance. The project is also financially supported by CTI, the Swiss Federal Commission for Technology and Innovation Grant N° 8330.2 EPRP-IW.

Nomenclature

Latin Symbols

A	Pipe cross section [m ²]	S_Q	Mass source [m ³ .s ⁻¹]
$C = \frac{gAdx}{a^2}$	Compliance [m ²]	S_h	Momentum source [m]
C_c	Cavitation compliance [m ²]	T	Temperature [K]
C_{equ}	Equivalent compliance [m ²]	U	Peripheral velocity [m·s ⁻¹]
D	Pipe diameter [m]	V_c	Cavitation volume [m ³]
D_{ref}	Reference diameter [m]	Z	Elevation [m]
$E = gH$	Machine specific energy [J·kg ⁻¹]	Z_{ref}	Elevation reference [m]
E_{wall}	Young modulus of the pipe wall [Pa]	a	Wave speed [m.s ⁻¹]
E_l	Bulk modulus of the liquid phase [Pa]	dx	Elementary pipe length [m]
H	Turbine head [m]	f	Frequency [Hz]
$L = \frac{dx}{gA}$	Hydraulic inductance [s ² .m ⁻²]	g	Gravitational acceleration [m·s ⁻²]
Q	Flow rate [m ³ .s ⁻¹]	h	Piezometric head [m]
$R = \frac{\lambda dx Q}{2gDA^2}$	Hydraulic resistance [s.m ⁻²]	n	Runner frequency [Hz]
R	Perfect gas constant [J.K ⁻¹ .mol ⁻¹]	p	Pressure [Pa]
R_{th}	Thermodynamic resistance [s·m ⁻²]	p_v	Vapor pressure [Pa]

Greek Symbols

β	Void fraction [-]	μ''	Bulk viscosity [Pa.s]
λ	Local loss coefficient [-]	Θ	Relaxation time [s]
ρ	Density, [kg.m ⁻³]	ω	Runner angular velocity [rad·s ⁻¹]
ρ_c	Cavitation density, [kg.m ⁻³]	σ	Thoma number [-]
$\varphi = \frac{8}{\pi} \frac{Q}{\omega D_{ref}^3}$	Flow coefficient [-]	$\psi = 8 \frac{E}{\omega^2 D_{ref}^2}$	Energy coefficient [-]

Subscripts, Superscripts, Acronyms

\tilde{y}	Quantity fluctuations	HD	Hydrodynamic
\bar{y}	Time averaged quantity	SPS	Single Phase Simulation
HA	Hydroacoustic	TPS	Two Phase Simulation

References

- [1] Dörfler, P., 1985, "Francis turbine surge prediction and prevention". In Proceedings of the Waterpower 85, Las Vegas, USA, pp. 1-10.
- [2] Dörfler, P., 1994, "Observation of the pressure pulsation on Francis model turbine with high specific speed". The International Journal of Hydropower and Dams, pp. 21-26.
- [3] Arpe, J., 2003, "Analyse du champ de pression pariétale d'un diffuseur coudé de turbine francis". Ph. D. Thesis, N°2779, EPFL, Lausanne, Switzerland.
- [4] Arpe, J., Nicolet, C. and Avellan, F., 2009. "Experimental Evidence of Hydroacoustic Pressure Waves in a Francis Turbine Elbow Draft Tube for Low Flow rate Conditions". Journal of Fluids Engineering, Vol 131, Issue 8, pp. 081102-1-9.
- [5] Nicolet, C., Arpe, J., and Avellan, F., 2004. "Identification and modeling of pressure fluctuations of a francis turbine scale model at part load operation". In Proceedings of the 22nd IAHR Symposium on Hydraulic Machinery and Systems, Stockholm, Sweden.
- [6] Koutnik, J., Faigle, P., and Moser, W., 2008. "Pressure fluctuations in Francis turbines-theoretical prediction and impact on turbine". In Proceedings of the 24th Symposium on Hydraulic machinery and Systems, Foz do Iguassu, Brazil.
- [7] Haban, V., Rudolf, P., Pochyly, F., Koutnik, J., and Krüger, K., 2007. "Stability of infinitely long asymmetrical vortex rope". In Proceedings of the 2nd International Meeting of Working Group on Cavitation and Dynamic Problems in Hydraulic Machinery and Systems, Timisoara, Romania.
- [8] Pochyly, F., Cermak, L., Rudolf, P., Haban, V., and Koutnik, J., 2009. "Assessment of the steady swirling flow stability using amplitude frequency characteristic". In Proceedings of the 3rd International Meeting of Working Group on Cavitation and Dynamic Problems in Hydraulic Machinery and Systems, Brno, Czech Republic.
- [9] Avellan, F., 2000, "Flow Investigation in a Francis Draft Tube: the Flindt Project". In Proceedings of XXth IAHR Symposium on Hydraulic Machinery and Systems, Charlotte, North California, USA.
- [10] Ciocan, G., Iliescu, M., Vu, T., Nennemann, B., and Avellan, F., 2007, "Experimental study and numerical simulation of the flindt draft tube rotating vortex". Journal of Fluids Engineering Vol 129, Issue 2, pp. 129-146.
- [11] Zobeiri, A., 2009, "Investigations of time dependent phenomena in a turbine and a pump turbine of Francis Type: rotor stator interactions and precessing vortex rope". PhD thesis, EPFL, Thèse N°4272.
- [12] Nicolet, C., 2007, "Hydroacoustic modelling and numerical simulation of unsteady operation of hydroelectric systems". Ph. D. Thesis, N° 3751, EPFL, Lausanne, Switzerland.
- [13] Wylie, E.B., Streeter, V.L. and Suo, 1993, "Fluid transients in systems". Prentice Hall.
- [14] Alligné, S., Nicolet, C., and Avellan, F., 2011, "Identification of Francis Turbine Helical vortex rope Excitation by CFD and Resonance Simulation with the Hydraulic System," In Proceedings of ASME-JSME-KSME Joint Fluids Engineering , Hamamatsu, Japan.
- [15] Ribner, H., 1964. "The generation of sound by turbulent jets," Advances in Applied Mechanics, Vol 8, pp. 103-182
- [16] Pezzinga, G., 2003, "Second viscosity in transient cavitation pipe flows". Journal of Hydraulic Research Vol 41, Issue 6, pp. 656-665.
- [17] Menter, F., 1994, "Two-equation eddy-viscosity turbulence models for engineering applications". AIAA journal, Vol 32, Issue 8, pp. 1598-1605.
- [18] Rath, H., 1981. "Unsteady pressure waves and shock waves in elastic tubes containing bubbly air-water mixtures," Acta Mechanica, Vol 38, Issue 1-2, pp. 1-17.
- [19] Alligné, S., Nicolet, C., Allenbach, P., Kawkabani, B., Simond, J.J., and Avellan, F., 2009, "Influence of the Francis turbine location under vortex rope excitation on the hydraulic system stability," International Journal of Fluid Machinery and Systems, Vol 2, Issue 4.